ISBN: 978-3-95450-248-6 ISSN: 2673-5490 doi: 10.18429/JACoW-IPAC2025-MOPS005

ADIABATIC CAPTURE IN HIGH INTENSITY, HIGH POWER RINGS

D. J. Kelliher*[1], C. Jolly[1,2], B. Kyle[1], J.-B. Lagrange[1], A. P. Letchford[1], S. Machida[1], A. Oeftiger[2], D.W. Posthuma de Boer[1,2], C. T. Rogers[1], A. Seville[1], R.E. Williamson[1]
[1] STFC Rutherford Appleton Laboratory, UK
[2] John Adams Institute, University of Oxford, Oxford, UK

Abstract

Finding the optimal RF voltage ramp to capture coasting beams in high intensity rings has been the subject of ongoing study for many decades. We are motivated to revisit the topic with a view to capturing coasting, stacked beams in a future high intensity, high power FFA. However, the results have general applicability. We compare various voltage laws including linear, bi-linear and iso-adiabatic through simulation and experiment, making use of the ISIS synchrotron. Using longitudinal tomography, we seek to establish the voltage program that minimises the captured beam emittance.

INTRODUCTION

Adiabatic capture refers to the process of capturing a coasting beam in an RF bucket with minimal (ideally zero) emittance growth. While direct capture of a chopped beam in a waiting RF bucket is normally preferred, there are situations where adiabatic capture is unavoidable or is advantageous. For example, in the case of beam stacking, it is necessary to capture the final stacked, coasting beam in order to create an abort gap for single-turn extraction. In that case, adiabatic capture minimises the required RF voltage and the longitudinal emittance of the captured beam.

Identifying the optimal functional form for the RF voltage ramp to achieve adiabatic capture has been the subject of debate for many decades. It has been reported that a linear voltage ramp leads to a poor result in terms of minimising the growth of the captured beam emittance, while quadratic or iso-adiabatic voltage ramps (where the adiabaticity is kept constant during the ramp) do better [1].

In this paper, we study adiabatic capture in high intensity, high power rings. We wish to minimise beam loss and optimise the voltage law. We are motivated by the case of beam stacking in a future high power FFA neutron spallation source, which is an option for ISIS-II [2]. In the absence of an existing high intensity FFA, experiments were carried out on the ISIS synchrotron.

To assess the effectiveness of the capture process, the emittance before and after the ramp should be measured. To measure the emittance of the coasting beam, the aim is to measure the Schottky noise. Longitudinal tomography is used to measure the captured beam emittance. In addition, the longitudinal tomography algorithm is used to reconstruct the distribution during capture.

* David.Kelliher@stfc.ac.uk

ADIABATIC CAPTURE THEORY

Consider a bunched beam contained in a RF bucket. If a longitudinal parameter such as the RF voltage changes, particles will follow fixed Hamiltonian contours so long as the timescale of the variation of the synchrotron tune is slow compared to the synchrotron period. This is expressed in terms of the adiabaticity parameter, ε

$$\varepsilon = \frac{2\pi}{\omega_s^2}\frac{d\omega_s}{dt} \tag{1}$$

where ω_s is the synchrotron frequency. The adiabaticity parameter should be small ($\varepsilon \ll 1$) in order for the process to be adiabatic. To maintain constant adiabaticity, the iso-adiabatic voltage law should be followed

$$U(t) = \frac{U_1}{1 - \frac{t}{t_f}\left(\frac{\sqrt{U_2}-\sqrt{U_1}}{\sqrt{U_2}}\right)} \tag{2}$$

where U_1, U_2 are the initial and final voltages and t_f is the duration of the capture process.

However, the idea that the adiabaticity should be kept constant is problematic when considering capture of a coasting beam. That is because the RF bucket separatrix sweeps across the beam during capture, and separatrix crossing is an inherently non-adiabatic process. Instead, it may be preferable for separatrix crossing to occur rapidly rather than slowly to minimise the disturbance to the beam.

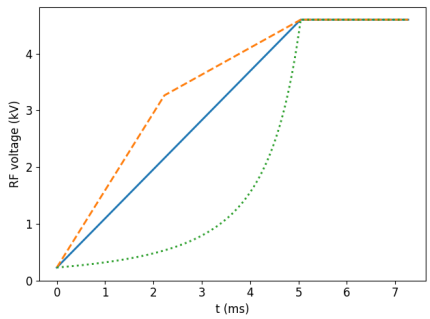

Figure 1: Comparison of linear (blue, solid), bilinear (orange, dashed) and iso-adiabatic (green, dotted) voltage ramps in the case where the ramp duration is 1 ms. In each case, the initial and final RF voltages are 0.2 kV and 4.6 kV, respectively.

EXTENDED LONGITUDINAL TOMOGRAPHY

In longitudinal tomography, the bunch distribution in longitudinal phase space (ϕ, δ) is reconstructed from the pro-

ISBN: 978-3-95450-248-6 ISSN: 2673-5490 doi: 10.18429/JACoW-IPAC2025-MOPS005

jections along the phase axis ϕ as the bunch rotates. The projections are given by the line density data measured by a diagnostic such as a wall current monitor or BPM. To reproduce the distribution accurately, the number of projections used in the reconstruction should encompass about half a synchrotron rotation.

The Algebraic Reconstruction Technique (ART) used in CT scans divides the image to be reconstructed into $m \times n$ pixels. The image x is found by solving

$$Ax = b \tag{3}$$

where b is the set of p measured projections, each comprising m bins and A is a $(p{\times}m){\times}(m{\times}n)$ coefficient matrix. An initial guess of x is made by back projection, which is given by the product of the inverse of A and b. A forward projection step is then made to calculate a new vector, b^{calc}. The difference between this and the measured b^{meas} is back projected and added to the initial x array. Iterations continue until the discrepancy between b^{calc} and b^{meas} converges.

In standard ART a rigid rotation of the object is assumed. In order to account for the non-rigid rotation of the distribution in the case of longitudinal phase space, the coefficient matrix A is computed by tracking particles starting in each pixel and noting the bin they fall into on each turn. This approach is adopted in the hybrid ART algorithm devised by S. Hancock [3]. This forms the basis of the tomography code used at CERN [4, 5].

If Eq. 3 is under-constrained, there are many possible solutions. The Maximum Entropy algorithm (MENT) attempts to find the solution with the highest multiplicity and therefore largest *a priori* probability, often resulting in fewer reconstruction artifacts. MENT does not require the explicit calculation of the matrix inverse [6].

In the CERN tomography code, the pixels are distributed within the RF bucket, meaning that nothing outside the bucket can be reconstructed. This is suitable if the distribution is completely captured in the RF bucket. In the present study, it is reasonable to make this assumption at the end of the voltage ramp when all or almost all the bunch is in the bucket. However, at the start of capture when the RF bucket area is zero or very small (in the case of finite initial voltage) the majority of the distribution is outside the bucket. Hence, in order to reconstruct the distribution at the start of capture (or during the capture process) we extend the solution space beyond the RF bucket.

EXPERIMENTAL SETUP

For these adiabatic capture experiments, the ISIS RCS is run in coasting beam mode. The intensity of the injected beam is around 2.2e12, which is a moderate level for ISIS. The phase of a debunching cavity in the injection linac can be adjusted to modify the injected beam momentum spread.

The voltage of a single RF cavity is ramped up in order to capture the beam following one of the voltage laws described above. Figure 1 shows the three voltage laws in the case of a 1 ms ramp. As can be seen in the figure, the voltage is kept constant for some time after the ramp in order to acquire data for tomography. The CT beam current monitor data is recorded along with beam loss monitors and BPMs (both vertical and horizontal).

Attempts to measure the coasting beam momentum spread via the Schottky noise were unsuccessful. This is because the frequency domain data was dominated by a coherent signal, masking the Schottky noise component.

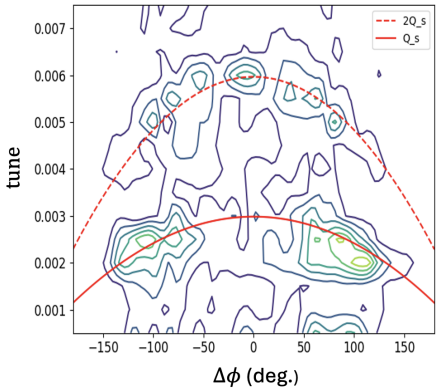

(a)

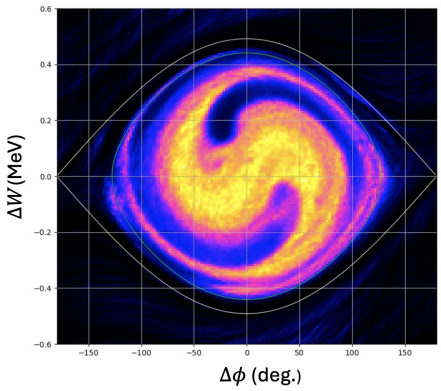

(b)

Figure 2: (a) Contour plot of the FFT amplitude of the BPM sum signal as a function of RF phase and synchrotron tune. The solid red and dashed red lines show the predicted synchrotron tune Q_s and $2Qs$ as a function of phase. (b) Corresponding reconstructed longitudinal phase space distribution. The 90% emittance is given by the area inside the green curve. In this case, the RF voltage is ramped linearly to 4.6 kV in 1 ms. The reconstruction is done after the ramp is complete.

RESULTS

The turn-by-turn line density data can be arranged into a 2D array with dimension $p \times m$ where m is the phase bin number and p is the turn number. By taking the FFT of each column, a contour plot can be produced which shows the frequency content of the distribution as a function of phase. Examination of the contour plot offers an insight into the dominant modes of the distribution even without recourse to tomography. In the example shown in Fig. 2a the strong signal at $2Q_s$ indicates a strong quadrupole component which

ISBN: 978-3-95450-248-6 ISSN: 2673-5490 doi: 10.18429/JACoW-IPAC2025-MOPS005

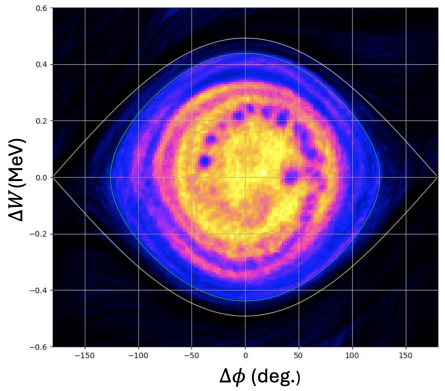

(a) Linear ramp

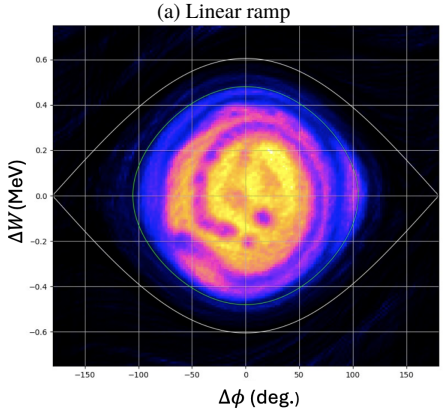

(b) Bilinear ramp

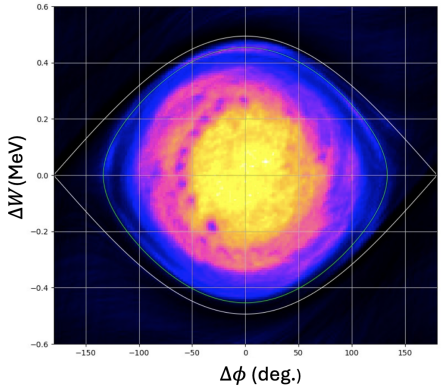

(c) Iso-adiabatic ramp

Figure 3: Reconstructed longitudinal phase space distributions for the case of three voltage laws. In all cases, the RF voltage is ramped to 4.6 kV. The reconstruction is done after the ramp is complete.

can also be seen in the reconstructed distribution, Fig. 2b. This occurs when the RF voltage is ramped rapidly during capture. On the other hand, the dipole component at Q_s indicates an offset between the RF frequency and the central revolution frequency of the coasting beam at the start of capture.

The distributions that result when the three different voltage laws are applied are compared in Fig. 3. The resulting emittances are given in Table 1. It can be seen that the emittance resulting from the iso-adiabatic ramp, Fig. 3c, is larger than the linear or bilinear cases (Figs. 3a and 3b).

Table 1: Captured Beam 90% Emittance (per Bucket) in the Case of Different RF Voltage Laws. In the Linear and Iso-Adiabatic Cases, the Final Voltage is 4.6 kV. In the Bilinear Case, the Voltage Ramps to 4.6 kV in 2 ms and then to 6.4 kV in 4 ms

Voltage law	Ramp time	Final emittance
Linear	5 ms	0.333 eV.s
Bilinear	6 ms	0.312 eV.s
Iso-adiabatic	5 ms	0.362 eV.s

In Fig. 4, the initial coasting beam distribution is reconstructed using the adapted longitudinal tomography code described above. The reconstruction is more challenging than in the bunched beam case, i.e. the discrepancy between b^{calc} and b^{meas} is higher. The diagonal line that appears in the upper left and lower right of the distribution appears to be an artifact of the separatrix that emerges as the RF voltage increases. The reconstructed distribution has a 90% momentum spread of $dp/p = \pm 0.0018$. This is consistent with other measurements of momentum spread at ISIS.

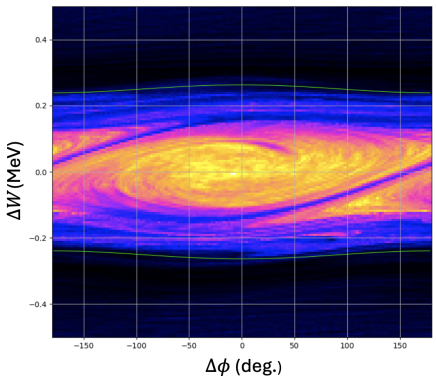

Figure 4: Reconstruction of the initial, coasting beam distribution at the start of capture. This is for the case of a 5 ms linear voltage ramp.

CONCLUSIONS

Although the results are not conclusive, they do suggest that a bilinear or linear voltage ramp outperforms an iso-adiabatic ramp in terms of the final captured beam emittance. Further work is required to reduce the coherent signal so that the Schottky noise can be measured. By extending the longitudinal tomography code, a reasonable reconstruction of the initial coasting beam was made.

REFERENCES

[1] S. Koscielniak and K. Zeno, "Adiabatic capture of longitudinal phase space", in *Proc. IPAC'23*, Venice, Italy, May 2023, pp. 3387–3390. doi:10.18429/JACoW-IPAC2023-WEPL118

[2] S. Machida, "FFA design study for a high intensity proton driver", in *Proc. IPAC'23*, Venice, Italy, May 2023, pp. 1437–1439. doi:10.18429/JACoW-IPAC2023-TUPA044

[3] S. Hancock, M. Lindroos, and S. Koscielniak, "Longitudinal phase space tomography with space charge", *Phys. Rev. ST*

ISBN: 978-3-95450-248-6 ISSN: 2673-5490 doi: 10.18429/JACoW-IPAC2025-MOPS005

Accel. Beams, vol. 3, p. 124202, 2000. doi:10.1103/PhysRevSTAB.3.124202

[4] C. Grindheim and S. Albright, "Longitudinal Phase Space Tomography Version 3", Rep. CERN-ACC-NOTE-2021-0004, Jan. 2021.

[5] https://tomograp.web.cern.ch

[6] C.T. Mottershead, "Maximum Entropy Beam Diagnostic Tomography", *IEEE Transactions on Nuclear Science*, vol. NS-32, no. 5, Oct. 1985.